

The following resources related to this article are available online at www.sciencemag.org (this information is current as of December 18, 2009):

Updated information and services, including high-resolution figures, can be found in the online version of this article at:

<http://www.sciencemag.org/cgi/content/full/279/5357/1672>

This article **cites 18 articles**, 4 of which can be accessed for free:

<http://www.sciencemag.org/cgi/content/full/279/5357/1672#otherarticles>

This article has been **cited by** 78 article(s) on the ISI Web of Science.

This article has been **cited by** 1 articles hosted by HighWire Press; see:

<http://www.sciencemag.org/cgi/content/full/279/5357/1672#otherarticles>

This article appears in the following **subject collections**:

Planetary Science

http://www.sciencemag.org/cgi/collection/planet_sci

Information about obtaining **reprints** of this article or about obtaining **permission to reproduce this article** in whole or in part can be found at:

<http://www.sciencemag.org/about/permissions.dtl>

March to mid-September of 1998.

Data collection during the aerobraking period. The atmospheric density of Mars at the aerobraking altitude showed significant variation over time as well as large orbit-to-orbit differences. On each orbit the density must be predicted to determine the appropriate and safe depth within the atmosphere for the aerobraking passage sufficiently in advance to command MGS to adjust its orbit. Although science data acquisition during the aerobraking phase was not in the original mission plan, MOC, TES, the accelerometer, the electron reflectometer, and the horizon sensor are all acquiring data to support density predictions. During the aerobraking passage through the atmosphere the spacecraft has the solar panels in

a V-configuration with the instrument panel in the lee direction. The accelerometer data is used to provide density profiles of this atmospheric passage. At the end of the aerobraking as the spacecraft exits the atmosphere it rolls to point the main antenna toward Earth. During this roll MOC and TES can obtain visual and thermal coverage of Mars. In addition, images from the Hubble Space Telescope and ground-based whole disk microwave observations are being utilized to predict changes in the atmospheric density.

REFERENCES AND NOTES

1. Mars Observer Special Issue, *J. Geophys. Res.* **97**, 7663 (1992).
2. An archive of the data sets used in the papers in this

issue is available as a CD-ROM and online through the Planetary Data System Geosciences Node HYPERLINK <http://www.pds.geo.wustl.edu>.

3. The Mars Surveyor '98 mission includes separate launches of the Mars climate Orbiter and the Mars Polar Lander. The New Millennium Mars Microprobe (DS2) is an experimental "hitchhiker" on the mission.
4. D. Smith *et al.*, *Science* **279**, 1686 (1998).
5. The authors are the Project Scientist (A.L.A.), Deputy Project Scientist (F.D.P.), and the Interdisciplinary Scientist responsible for Data Archiving (R.E.A.) for the Mars Global Surveyor Mission. We are indebted to engineers at the Jet Propulsion Laboratory and LMA who have devoted themselves to this mission over the years and who operate the spacecraft today. Our special acknowledgement goes to Glen Cunningham, Project Manager. Portions of the work described in this paper were performed by the Jet Propulsion Laboratory under contract to the National Aeronautics and Space Administration.

21 January 1998; accepted 18 February 1998

The Structure of the Upper Atmosphere of Mars: In Situ Accelerometer Measurements from Mars Global Surveyor

G. M. Keating,* S. W. Bougher, R. W. Zurek, R. H. Tolson, G. J. Cancro, S. N. Noll, J. S. Parker, T. J. Schellenberg, R. W. Shane, B. L. Wilkerson, J. R. Murphy, J. L. Hollingsworth, R. M. Haberle, M. Joshi, J. C. Pearl, B. J. Conrath, M. D. Smith, R. T. Clancy, R. C. Blanchard, R. G. Wilmoth, D. F. Rault, T. Z. Martin, D. T. Lyons, P. B. Esposito, M. D. Johnston, C. W. Whetzel, C. G. Justus, and J. M. Babicke

The Mars Global Surveyor (MGS) z-axis accelerometer has obtained over 200 vertical structures of thermospheric density, temperature, and pressure, ranging from 110 to 170 kilometers, compared to only three previous such vertical structures. In November 1997, a regional dust storm in the Southern Hemisphere triggered an unexpectedly large thermospheric response at mid-northern latitudes, increasing the altitude of thermospheric pressure surfaces there by as much as 8 kilometers and indicating a strong global thermospheric response to a regional dust storm. Throughout the MGS mission, thermospheric density bulges have been detected on opposite sides of the planet near 90°E and 90°W, in the vicinity of maximum terrain heights. This wave 2 pattern may be caused by topographically-forced planetary waves propagating up from the lower atmosphere.

The Mars thermosphere is that portion of the upper atmosphere where the global mean temperatures increase with height above a minimum (~120 K) at altitudes of 100 to 120 km to maximum values of 200 to 350 K above 150 km. At the greater heights, the thermosphere is dominated by the absorption of extreme ultraviolet (EUV) solar radiation and by the diffusive separation of individual gases such as CO₂, O, N₂, and CO (1). Variability in the thermosphere reflects diurnal, seasonal, and solar cycle variations in the solar flux at Mars (2) and in the ability of energy to propagate upward from the lower atmosphere (that is, from below 100 km). This coupling of Mars' atmospheric regions is particularly affected

by atmospheric heating (3) and dynamic forcing in response to changes in the amount of dust in the atmosphere (4). Overall, the expansion and contraction of the Mars lower atmosphere is controlled by several processes that are difficult to separate: (i) dust heating, (ii) solar infrared (IR) heating that varies with the Mars heliocentric distance, and (iii) various dynamic influences such as gravity waves, planetary waves, and tides.

Previous in situ measurements from Viking Landers 1 and 2 and Mars Pathfinder (5), and remote sensing measurements of air glow, plasma and neutral density scale heights, and monitoring of the altitude of the F1-peak in electron density (1, 6) have

only partially characterized these thermospheric variations because of the limited coverage in space and time. Now, measurements from the z-axis accelerometer aboard MGS (7) have yielded to date more than 200 vertical structures of thermospheric density and derived temperature and pressure. These data have been obtained at successive MGS periapses over a 5-month period spanning northern fall on Mars ($L_s = 180^\circ$ to 270°) (8), from September 1997 to February 1998, as MGS continues aerobraking into its mapping orbit (9). During the mission the spacecraft periapsis has moved from 32°N to 50°N and from a local solar time (LST) of 6 p.m. to noon, with data acquired from 170 km to as low as 110 km.

The MGS z-axis accelerometer, aligned closely to the spacecraft velocity vector (v), measures the drag force acceleration (a), related to atmospheric density (ρ) by the classical relation:

$$\rho = [2m/v^2 C_D s] a \quad (1)$$

with spacecraft mass (m), cross-sectional area (s) relative to v , and drag coefficient

G. M. Keating, R. H. Tolson, G. J. Cancro, S. N. Noll, J. S. Parker, T. J. Schellenberg, R. W. Shane, B. L. Wilkerson, The George Washington University at NASA Langley, MS 269, Hampton, VA 23681, USA.

S. W. Bougher and J. M. Babicke, University of Arizona, Tucson, AZ 85721, USA.

R. W. Zurek, T. Z. Martin, D. T. Lyons, P. B. Esposito, M. D. Johnston, C. W. Whetzel, Jet Propulsion Laboratory, California Institute of Technology, Pasadena, CA 91109, USA.

J. R. Murphy, J. L. Hollingsworth, R. M. Haberle, M. Joshi, NASA Ames Research Center, Moffett Field, CA 94035, USA.

J. C. Pearl, B. J. Conrath, M. D. Smith, NASA Goddard Space Flight Center, Greenbelt, MD 20771, USA.

R. T. Clancy, Space Science Institute, Boulder, CO 80309, USA.

R. C. Blanchard, R. G. Wilmoth, D. F. Rault, NASA Langley Research Center, Hampton, VA 23681, USA.

C. G. Justus, Computer Sciences Corporation, Huntsville, AL 35824, USA.

*To whom correspondence should be addressed.

(C_D). The z -accelerometer (10) is 38 times more sensitive (0.332 mm/s per count) than the Viking entry accelerometers (11) allowing measurements up to at least 170 km. Accelerometer measurements sensitive to the thermosphere are generally obtained from 200 s before periapsis to 200 s after periapsis, a span of about 30° in latitude. Additional accelerometer measurements are obtained before and after this period to determine accelerometer bias for each pass. Measurements are obtained every 0.1 s. Inbound atmospheric measurements were north of periapsis, and outbound to the south. Extraneous accelerations associated with spacecraft thruster activity and angular accelerations were removed. Using spacecraft pointing knowledge, C_D was determined through an iterative process that accounts for the transitional regime between free molecular and continuum flow (12). Densities and scale heights were determined over 6-s running means to filter out 6-s oscillations of the spacecraft or 40-s running means to filter out atmospheric wave activity to better estimate mean structure. Accelerations of one micro-g were detected. Overall, random errors in density were estimated to be less than 3% at altitudes below 140 km. At higher altitudes uncertainties in accelerometer measurement bias dominate error estimates. Systematic uncertainties in C_D of less than 10% do not significantly affect measurements of relative variations, such as wave activity.

Thermospheric structure. Thermospheric densities measured by the MGS accelerometer at the evening terminator near the start of aerobraking were close to the late afternoon Viking 1 densities (Fig. 1), but at 130 km were a factor of 4.5 higher than the corresponding pre-dawn Mars Pathfinder values (5). Seasonal and diurnal variations should contribute to this difference (13). Simulations by a coupled Mars General Circulation Model (MGCM) and Mars Thermospheric Global Circulation Model (MTGCM) (14) indicate that the density difference between MGS and Mars Pathfinder can largely be accounted for by a factor of 2 increase in density due to seasonal variation ($L_s = 143^\circ$ to 190°), and a doubling due to diurnal variation within the thermosphere (3 a.m. to 6 p.m.), assuming a visible dust opacity level between 0.3 and 1.0. Using the MGCM-MTGCM model to adjust the Viking 1 thermospheric data to the MGS periapsis latitude, LST, solar activity level, L_s (8), and Mars-sun distance, the thermospheric densities in the Viking 1 era are estimated to be more than a factor of 2 higher than these MGS values. This is primarily due to the large differences in the Mars-sun distance between the two

thermospheric data sets. Thus, the close overlap of these two thermospheric density profiles (Fig. 1) may be associated with long-term climate variations (1977 to 1997), differences in opacity (15), natural variability, or a combination of all three sources.

The MTGCM simulations reflect a boundary forcing based on the MGCM simulations of the lower atmosphere for specified dust opacities. Currently, only zonally averaged height and temperature fields and specific (semi-diurnal) components of the LST variation of the geopotential field are included. In absolute terms, densities obtained from the MGS accelerometer generally exceeded the unadjusted MTGCM values by 50 to 100%. These underestimates of densities are equivalent to a 3- to 5-km offset of the model and actual thermosphere heights. To remove this bias, given the current inability to validate the model temperature fields between about 70 km and periapsis altitudes, the MGCM zonally-averaged heights used at the MTGCM lower boundary (1.32- μ bar level) are offset up to 5 km to obtain the MGS accelerometer measured height of the 1.26-nbar level in the thermosphere (16).

MGS-derived temperatures above 150 km from accelerometer-derived scale heights appear to asymptote to values near 200 K. The vertical temperature structures, derived from scale heights and estimates of mean molecular weight, are in general accord with MTGCM temperatures of the upper thermosphere for visible dust opaci-

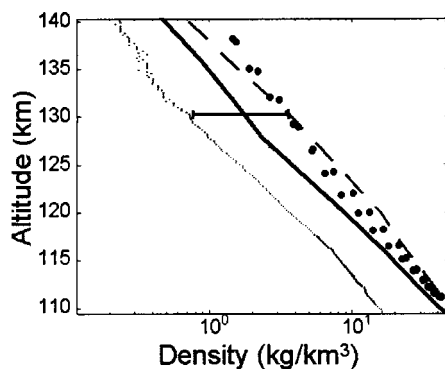


Fig. 1. MGS accelerometer data between 110 and 140 km (solid circles) for P012 (1 October 1997), taken at LST = 17:54 and $L_s = 190^\circ$ compared with previous in situ martian thermosphere density measurements (5). Dashed line represents data from Viking 1, taken at LST = 16:13 and $L_s = 100^\circ$. Heavy solid line represents data from Viking 2 at LST = 9:49 and $L_s = 120^\circ$. Thin dotted line on left shows data from Mars Pathfinder at LST = 3:00 and $L_s = 143^\circ$. Horizontal line shows estimate of change between Mars Pathfinder and MGS values due to seasonal and diurnal differences based on MTGCM calculations.

ties of 0.3 and 1.0. However, observed scale height derived temperatures at 130 km are colder than the MTGCM model predictions (120 K versus 150 K), even with the altitude adjustment described previously. These colder temperatures appear to be a general characteristic of the Mars lower thermosphere. The MTGCM takes into account the present low solar activity, but may underestimate CO_2 15- μ m cooling (2, 17). Specifically, a larger O/ CO_2 mixing ratio would lead to an enhancement of CO_2 cooling, as for Venus. This O/ CO_2 ratio is presently uncertain for Mars by at least a factor of 2. Gravity wave processes may also not be represented adequately in the models and could contribute to the temperature discrepancy.

MGS accelerometer measurements of atmospheric density obtained in the upper thermosphere at 160 km (November 1997 to January 1998) (Fig. 2) are different on inbound and outbound. Densities to the south exceed those to the north in every case. On the average, the densities during this northern fall season increase from 57°N to 33°N by 75%. Comparable values simulated by the MTGCM are about 66%, in agreement with observations. The latitudinal variations in the upper thermosphere may be largely due to changing solar extreme ultraviolet radiation (EUV) input with solar zenith angle and changing conditions at lower altitudes. In the lower thermosphere at 130 km, densities are occasionally higher to the north.

Two increases in density were observed at 160 km, one maximum in density after periapsis 50 (P050) and the second maximum in density after P090 (Fig. 2). The first peak is apparently related to a local dust storm and the second feature may be caused by an increase in EUV from the sun. The 10.7 cm solar flux, which is routinely used

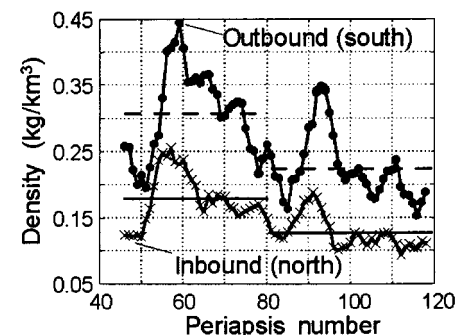


Fig. 2. Five-orbit running means of thermospheric densities measured by the MGS accelerometer at 160 km from November 1997 through January 1998 north (inbound) and south (outbound) of periapsis, separated on average by 24° in latitude. Horizontal lines show mean inbound (solid line) densities and outbound (dotted line) before and after P080.

as a proxy to estimate solar EUV radiation variations, reaches a local maximum, when viewed from Earth 17 days before P093, when 160 km densities maximized. With the 27-day rotation period of the sun, this face of the sun would be seen at Mars 17 days later near the time of P093. Such atmospheric responses may have been previously obscured by the dust storm. The response is not indicated in the lower thermosphere (Fig. 3), due to much weaker solar EUV effects at these lower altitudes. Such possible 27-day variations in the thermosphere, related to the 27-day rotation of the sun, have been detected previously in the Venus thermosphere (18).

Thermospheric storms. The MGS accelerometer observed two episodes of prolonged and substantial increase in lower thermospheric density. The first occurred on P015, with a 50% increase in atmospheric density at 110 km altitude. Measurements on P016 to P018, taken near 121 km, showed further increases of 60 to 90% as compared to earlier orbits near that altitude, indicating that the P015 event was not short-lived.

An even larger density increase occurred on P051 (130%), after detection by the MGS Thermal Emission Spectrometer (TES) (18) two orbits earlier (P049, $L_s = 224^\circ$, 25 November 1997) of a fully developed regional dust storm in the southern hemisphere Noachis Terra region (initially centered near 40°S , 20°E). Past data indicate that such storms are likely to occur on Mars during southern spring and summer, particularly during $L_s = 200^\circ$ to 330° (4).

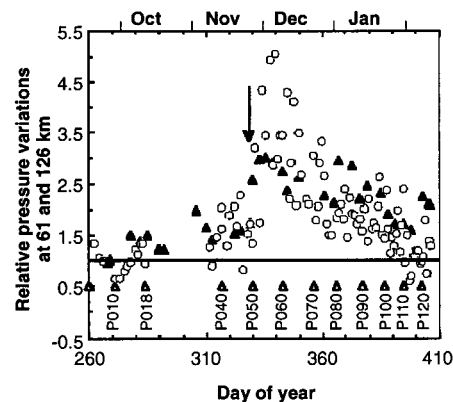


Fig. 3. Change in pressure with time (and MGS orbit number) at reference altitudes of 61 and 126 km and normalized to values on 26 September 1997, as derived from ground-based Mars disk-averaged microwave data (15, 28) (solid triangles), also normalized by surface pressure estimates. The microwave data are compared to 126 km MGS accelerometer data (open circles). Arrow indicates first detection of Noachis dust storm by MGS. Open triangles indicate even-numbered periapsis pressures and are labeled below the symbol.

In both cases, density increases coincided with warming and hydrostatic expansion of the lower atmosphere. In Fig. 3, periapsis densities have been converted to pressure at a common reference altitude of 126 km using atmospheric scale heights derived from MGS accelerometer data. These values are compared to pressures at a reference level of 61 km, estimated by using vertical profiles of temperature (as a function of pressure) derived from microwave (MW) spectrometer measurements of thermal emission in the 230 GHz CO line (15). The ground-based MW spectrometers average over the whole disk of Mars visible to the Earth observatory and so are representative of widespread changes, while the accelerometer measurements are specific to latitudes near periapsis between 32° and 50°N . The microwave and accelerometer data sets show similar trends, especially the onset of the dust storm in late November followed by its gradual decline. The stronger response in the thermosphere to the dust storm may be due to additional warming in the 70- to 120-km region which is not directly observed. The delay of increase in periapsis density by 2 to 3 days following the onset of the Noachis storm probably reflects the remote northern location of the aerobraking periapses.

Rapid increases in atmospheric temperatures have been seen in microwave data acquired in previous Mars years, particularly above 30 km (15). Such increases are attributed to changes in atmospheric dust loading, based on previous spacecraft data, together with radiative and radiative-dynamical modeling of the effects of dust heating of the atmosphere (3, 4). However, no dust storm activity was detected during the P015–P018 period by TES (18) or the MGS Mars Orbiter Camera (MOC) (19), although their coverage was restricted largely to the Southern Hemisphere. Full disk views on 5 October (P014) and 9 (P016–017) by the Hubble Space Tele-

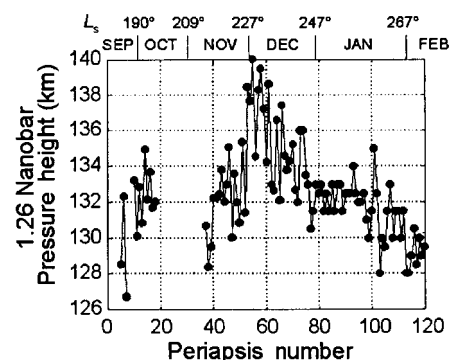


Fig. 4. The 1.26 nanobar pressure height (km) measured by the MGS accelerometer.

scope (HST) (20) also showed no significant dust activity or change (21). HST images were obtained until mid-October when the planet moved too close to the sun for safe viewing by HST. Meanwhile, column opacity estimates from the Imager for Mars Pathfinder (22) had also stopped with that mission's end in September.

By contrast, TES and MOC observed the Noachis regional dust storm (18, 19), and TES observations showed that by P052, 3 days after the storm was detected, the dust opacity in northern mid-latitudes had doubled. This is consistent with the higher temperatures seen by TES (increases >10 K) in both hemispheres, the ground-based MW data (Fig. 3), and increased thermospheric densities measured by the MGS accelerometer. The storm is classified as "regional" because the area of high opacity (>1) remained confined to Noachis and adjacent regions.

MGS measured heights of the 1.26-nbar level showed a general upward trend as perihelion (near southern summer solstice) approached and sharp increases (up to 140 km) during the Noachis dust storm (Fig. 4). This height is a rough measure of the integrated thermal structure of the lower atmosphere and reflects changing seasonal IR and dust storm heating of the lower atmosphere (17).

The trend from 128 to 132 km of the 1.26-nbar height before the dust storm (before P049) is close to that expected for this season (16). The orbit-to-orbit fluctuations seen reflect the MGS densities measured at thermospheric altitudes (Fig. 4). Post-dust storm heights are seen to dip below 132 km as the MGS periapsis moved northward. Thermospheric densities had largely returned to seasonal values by early January ($L_s = 250^\circ$; P085), while dust visual opacities estimated from TES data had declined from values greater than 1 to typically 0.5 or less (18).

The passage of a dust storm event and its effects on the thermosphere were also mon-

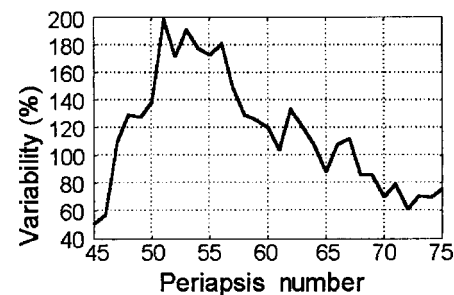


Fig. 5. The two standard deviation thermospheric disturbance levels (%) as defined in the text and as measured by the MGS accelerometer. In log space, a plus log residual of 200% corresponds to a minus log residual of 67%.

itored by tracking the thermospheric variability, measured by the MGS accelerometer, with time (Fig. 5). The ratio of the thermospheric density measured on any given pass to the density measured on the previous pass (adjusted for altitude using the observed scale heights) was used as an indicator of the atmospheric disturbance level. The “variability” parameter plotted is the $2\text{-}\sigma$ percent deviation of the logs of these ratios using the present ratio and the previous four ratios. Thermospheric disturbances sharply increased on P047 from 60% to over 100% before the initiation of the dust storm on P049. Maximum disturbances of 200% occurred on P051. The thermospheric disturbance level gradually decayed between P052 and P075 back toward pre-storm values of about 60%. These pre-storm and post-storm disturbance levels are consistent with prior estimates of short-term variability of the Mars thermosphere estimated using the Mariner 9 (M9) radio occultation data (16), which did not cover the onset of the 1971 global dust storm.

Planetary waves. A large part of the orbit-to-orbit variability observed with the MGS accelerometer is due to a stationary planetary-scale variation with longitude at thermospheric altitudes (110 to 170 km). Harmonic analysis of the longitudinal variations in densities were obtained from 14 accelerometer data sets, each with good longitudinal sampling (typically 10 orbits), and adjusted to a common altitude of 125 km (23). This analysis revealed a wave 2 pattern, which is a two-cycle wave over 360° of longitude. This wave 2 is essentially fixed in longitude, but varying in amplitude throughout the MGS aerobraking mission. One minimum of this wave 2 pattern always occurred near the central meridian, from 16°E to

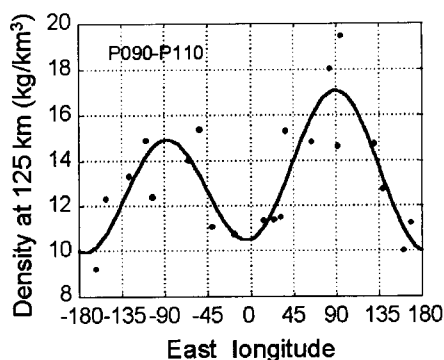


Fig. 6. Thermospheric density, normalized to 125 km, as a function of East longitude (solid circles) measured from P090 through P110 by the MGS accelerometer. The solid curve represents a least-mean-square fit solving for wave 1 and wave 2. For this case, wave 1 has an amplitude (mean to peak) of 8% of the mean and a phase (for the minimum) of 256°E , and wave 2 has an amplitude of 22% of the mean and a phase of 1°E .

18°W with an average phase of 2°E . Figure 6 shows the combined wave 1 and wave 2 variation during a non-dust storm time period (P090–P110). In most cases wave 2 was stronger than wave 1, and wave 1 was not stationary. During the initiation of the dust storm the wave 2 percent amplitude increased to $\pm 39\%$ compared to mission mean levels of $\pm 22\%$. Through additional harmonic analyses, the standing wave 2 phenomena was also detected in the 1.26 nbar levels, 160 km densities, and conditions at 130 km.

The persistence of this wave 2 pattern with its nearly constant phase suggests a forcing continuous in time related to surface topographic forcing. MGS periapses have spanned the latitude range 32°N to 50°N during fall and early winter. Mars’ surface topography exhibits significant longitudinal variability at the MGS periapsis latitudes (32°N to 50°N) (24) with a substantial wave 2 component (± 2 km) due to the Tharsis and Arabia highlands. Low-level eastward winds at northern middle latitudes during northern autumn and winter can interact with this topography and excite vertically propagating planetary-scale waves. The ability of these waves to propagate all the way into the thermosphere depends on the presence of eastward zonal winds in the lower atmosphere. Such winds are inferred up to at least 50 km from the TES temperature cross-sections (18).

MGCM results suggest that waves 1 and 2 can be topographically forced during northern fall and winter and can propagate to above 80 km (25). Vertical propagation above these altitudes depends upon the winds at higher altitudes. The robust planetary-wave pattern seen in the thermosphere in the accelerometer data indicates that, unlike Earth, the eastward moving winds present in northern mid-latitude during the fall do not close off (that is, decrease to zero wind speed or reverse direction) below the thermosphere, thereby permitting strong planetary waves to propagate into the thermosphere.

These thermospheric measurements from the MGS accelerometer, coupled with simultaneous lower atmosphere measurements, provide a quantitative means to examine the coupling of these atmospheric regions. The physical mechanisms responsible for this coupling can be compared to those known to operate for Earth. These results may also benefit future Mars missions that will rely on aerobraking or aerocapture.

REFERENCES AND NOTES

- C. A. Barth *et al.*, in *Mars*, H. H. Kieffer, B. M. Jakosky, C. W. Snyder, M. S. Matthews, Eds. (Univ. of Arizona Press, Tucson, 1992), pp 1054–1089.
- S. W. Bougher, D. M. Hunten, R. G. Roble, *J. Geophys. Res. Planets* **99**, 14609 (1994).
- R. W. Zurek *et al.*, in *Mars*, H. H. Kieffer, B. M. Jakosky, C. W. Snyder, M. S. Matthews, Eds. (Univ. of Arizona Press, Tucson, 1992), pp 835–933.
- R. Kahn *et al.*, in *Mars*, H. H. Kieffer, B. M. Jakosky, C. W. Snyder, M. S. Matthews, Eds. (Univ. of Arizona Press, Tucson, 1992), pp 1017–1053; L. J. Martin and R. W. Zurek, *J. Geophys. Res.* **97**, 3221 (1993).
- A. Seiff and D. B. Kirk, *J. Geophys. Res.* **82**, 4364 (1977); A. O. Nier and M. B. McElroy, *J. Geophys. Res.* **82**, 4341 (1977); J. T. Schofield *et al.*, *Science* **278**, 1752 (1997).
- A. I. F. Stewart and W. B. Hanson, *Adv. Space Res.*, **2**, 87 (1982); A. J. Kliore *et al.*, *J. Geophys. Res.* **78**, 4331 (1973).
- G. M. Keating *et al.*, *Eos* **78**, 48, F401, (1997). G. M. Keating, R. H. Tolson, S. W. Bougher, R. C. Blanchard, MGS Accelerometer Proposal for JPL Operations (1995).
- Aerocentric longitude of the sun, L_s , is used as an angular measure of the Mars year: $L_s = 0, 90, 180, 270$ corresponds to the start of northern spring, summer, fall, and winter, respectively.
- A. L. Albee, F. D. Palluconi, R. E. Arvidson, *Science* **279**, 1671 (1998).
- The Sundstrand QA 1200 accelerometer, contained in the MGS Inertial Reference Unit package is thermostatically controlled to maintain an internal temperature to within 0.12 K. This has resulted in the temperature-sensitive bias of the z-accelerometer being highly stable, to within a small fraction of 1% throughout the aerobraking phase.
- R. C. Blanchard and G. D. Walberg, *NASA Tech. Pap.* 1793 (1980).
- R. W. Shane, D. F. G. Rault, R. H. Tolson, *Am. Inst. Aeronautics Astronautics* **97**, 2509 (1997).
- S. W. Bougher *et al.*, *J. Geophys. Res.* **95**, 1,811 (1990); S. W. Bougher *et al.*, *ibid.* **98**, 3281 (1993); S. Bougher, *Adv. Space Res.* **15**, 21 (1995).
- S. W. Bougher, J. M. Murphy, R. M. Haberle, *Adv. Space Res.* **19**, 1255 (1997). The NASA Ames Mars General Circulation Model (MGCM) extends from the surface to 0.2 microbar (near 100 km) (26). The NCAR/University of Arizona Mars Thermospheric Global Circulation Model (MTGCM) covers the altitude range 70 to 300 km (13). Coupling between the two models was accomplished by passing zonally averaged mean temperatures and geopotential heights from the MGCM to the MTGCM lower boundary at the 1.32 μbar level. Also included in this MGCM-MTGCM coupling are the geopotential heights and corresponding phases of five semidiurnal tidal components, representing a principal mode of local solar time dynamical forcing of the thermosphere.
- R. T. Clancy, D. O. Muhleman, G. L. Berge, *J. Geophys. Res.* **95**, 14543 (1990); R. T. Clancy *et al.*, *Icarus* **122**, 36 (1996). MW data was recorded at the Mauna Kea James Clerk Maxwell Telescope and the Kitt Peak National Astronomical Radio Observatory.
- The 1.26-nbar (nanobar) reference level corresponds to the height of the main ionospheric (F1-layer) peak at the subsolar point (6). A. I. F. Stewart derived systematic trends in the height of the 1.26 nbar pressure level based on Mariner 9 and Viking radio occultation data (27) and then estimated (Internal JPL Report) a short-period (orbit-to-orbit) variation of ± 2.8 km as a root-mean-squared residual. Assuming a 7.5-km atmospheric scale height, this indicated a variability of $\pm 35\%$ (1σ). The height scale for the MTGCM model is calibrated using this 1.26-nbar level height as a local reference level.
- G. M. Keating and S. W. Bougher, *Adv. Space Res.* **7**, 57 (1987); *J. Geophys. Res.* **97**, 4189 (1992).
- P. R. Christensen *et al.*, *Science* **279**, 1693 (1998).
- M. Malin *et al.*, *ibid.*, p. 1681 (1998).
- P. B. James *et al.*, *Icarus* **109**, 79 (1994).
- P. B. James, private communication.
- P. H. Smith *et al.*, *Science* **278**, 1768 (1997).
- The results of the harmonic analyses of MGS accelerometer densities normalized to 125 km for the phase of wave 2 (measured from wave 2 minimum) for the mission through P114 are as follows: 1.

Passes 10–18 (P010–P018), longitude of the wave 2 minimum -14°E ; 2. P037–P046, $+3^{\circ}\text{E}$; 3. P040–P049, $+3^{\circ}\text{E}$; 4. P045–P054, $+16^{\circ}\text{E}$; 5. P050–P059, $+15^{\circ}\text{E}$; 6. P055–P064, $+13^{\circ}\text{E}$; 7. P060–P069, -12°E ; 8. P065–P074, -3°E ; 9. P070–P079, -8°E ; 10. P068–P094, -18°E ; 11. P090–P099, -3°E ; 12. P095–P104, 1°E ; 13. P100–P109, -3°E ; 14. P105–P114, 8°E . The mean phase ± 1 standard deviation for the 14 cases is $2^{\circ}\text{E} \pm 10^{\circ}$ (for the wave 2 minimum). Variations in the time intervals of analysis is required to obtain

longitudinal coverage for changing orbital periods.
 24. G. Balmino, G. Moynot, N. Vales, *J. Geophys. Res.* **87**, 9735 (1982). D. E. Smith, and M. T. Zuber, *Science* **271**, 184 (1996).
 25. J. R. Barnes *et al.*, *J. Geophys. Res.* **101**, 12753 (1996). J. L. Hollingsworth and J. R. Barnes, *J. Atmos. Sci.* **53**, 428 (1996).
 26. J. B. Pollack *et al.*, *J. Geophys. Res.* **95**, 1447 (1990); J. R. Murphy *et al.*, *ibid.* **100**, 26357 (1995).
 27. A. I. F. Stewart, *LASP-JPL Internal Rep.*, PO# NQ-

802429, Jet Propulsion Laboratory, Pasadena, CA, March (1987).

28. R. T. Clancy and B. Sandor, private communication.
 29. We thank the Mars Surveyor Operations Project at Jet Propulsion Laboratory (JPL) and the MGS spacecraft operations team at Lockheed Martin Astronautics (Denver, CO) for their support in providing the MGS Accelerometer Team with the accelerometer and ancillary data used in this study. This work was funded in part by the JPL, Pasadena, CA.

20 January 1998; accepted 13 February 1998

Magnetic Field and Plasma Observations at Mars: Initial Results of the Mars Global Surveyor Mission

M. H. Acuña, J. E. P. Connerney, P. Wasilewski, R. P. Lin, K. A. Anderson, C. W. Carlson, J. McFadden, D. W. Curtis, D. Mitchell, H. Reme, C. Mazelle, J. A. Sauvaud, C. d'Uston, A. Cros, J. L. Medale, S. J. Bauer, P. Cloutier, M. Mayhew, D. Winterhalter, N. F. Ness

The magnetometer and electron reflectometer investigation (MAG/ER) on the Mars Global Surveyor spacecraft has obtained magnetic field and plasma observations throughout the near-Mars environment, from beyond the influence of Mars to just above the surface (at an altitude of ~ 100 kilometers). The solar wind interaction with Mars is in many ways similar to that at Venus and at an active comet, that is, primarily an ionospheric-atmospheric interaction. No significant planetary magnetic field of global scale has been detected to date ($< 2 \times 10^{21}$ Gauss-cubic centimeter), but here the discovery of multiple magnetic anomalies of small spatial scale in the crust of Mars is reported.

The Mars Global Surveyor (MGS) magnetic field experiment is identical to that developed for the Mars Observer Mission that failed to achieve Mars orbit in 1993 (1). The instrumentation provides fast vector measurements (up to 16 samples per second) of magnetic fields over a dynamic range of 0.005 to 65,536 nT per axis. The fundamental objectives of this investigation are to establish the nature of the magnetic field of Mars, to develop appropriate models

for its representation, and to map the crustal remnant field to a resolution consistent with spacecraft orbit altitude and ground track separation. The instrument complement includes two redundant triaxial fluxgate magnetometers and an electron reflectometer (1). The vector magnetometers provide in situ sensing of the ambient magnetic field in the vicinity of the MGS spacecraft over the automatically selected full-scale ranges of ± 4 nT to $\pm 65,536$ nT, with a digital resolution of 12 bits. The electron reflectometer measures the local electron distribution function in the range of ~ 1 eV to 20 KeV and will remotely sense the strength of the magnetic field down to the top of the martian atmosphere using directional information provided by the vector magnetometer. This synergistic combination was designed to increase the sensitivity and spatial resolution achievable from martian orbit with the vector magnetometer alone. Electron reflection magnetometry was first used on measurements from Apollo 15 and 16 Particles and Fields subsatellites (2).

Unlike Mars Observer, MGS lacks a boom to separate sensors from the spacecraft body to reduce interference by space-

craft-generated magnetic fields. Instead, each magnetometer sensor is placed at the outer edge of the articulated solar panels, about 5 m from the center of the spacecraft bus. The electron reflectometer sensor is mounted directly on the spacecraft nadir panel. This "twin magnetometer" configuration does not allow the real-time estimation of spacecraft fields (3) but provides redundancy and the near real-time detection and identification of spacecraft-generated magnetic fields. This instrument configuration required the design and implementation of magnetically "clean" solar array panels, which are used for aerobraking of the MGS spacecraft to achieve the final mapping orbit and are articulated about two orthogonal axes with respect to the spacecraft bus. Therefore, the orientation of the magnetic field sensors with respect to the spacecraft is variable and follows that of the solar panels, which are controlled to satisfy a variety of engineering requirements. The estimated accuracy of the measurements reported here is ± 0.5 nT before and after reconfiguration of the spacecraft for aerobraking, and ± 3 nT during the aerobraking phase. The magnetometer and electron reflectometer (MAG/ER) designs have extensive space flight heritage, and similar versions have been flown in numerous planetary and space physics missions. The instrument is operating nominally, and 2 to 16 vector samples per second of magnetic field data are acquired, depending on the telemetry rate supported by the telecommunication system.

The MGS spacecraft was inserted initially into a highly elliptical orbit with apoapsis > 10 Rm (1 Rm = Mars equatorial radius = 3397 km) and periapses as low as 112 km above the surface. The significant advantages of aerobraking orbits to the MAG/ER investigation were recognized early in the planning of the observations. In these orbits the spacecraft dips below the bottom of the martian ionosphere, allowing the MAG/ER experiment to achieve high sensitivity and spatial resolution for the detection of weak crustal fields. In addition, high plasma densities expected at these low altitudes required a different measurement technique, so a Langmuir probe operational

M. H. Acuña, J. E. P. Connerney, P. Wasilewski, NASA Goddard Space Flight Center, Greenbelt, MD 20771, USA.

R. P. Lin, Space Sciences Laboratory and Department of Physics, University of California, Berkeley, CA 94720, USA.

K. A. Anderson, C. W. Carlson, J. McFadden, D. W. Curtis, D. Mitchell, Space Sciences Laboratory, University of California, Berkeley, CA 94720, USA.

H. Reme, C. Mazelle, J. A. Sauvaud, C. d'Uston, A. Cros, J. L. Medale, Centre d'Etude Spatiale des Rayonnements, 31209 Toulouse Cedex, France.

S. J. Bauer, University of Graz and Space Research Institute, A-8010 Graz, Austria.

P. Cloutier, Department of Space Physics and Astronomy, Rice University, Houston, TX 77005, USA.

M. Mayhew, National Science Foundation, Arlington, VA 22230, USA.

D. Winterhalter, Jet Propulsion Laboratory, California Institute of Technology, Pasadena, CA 91109, USA.

N. F. Ness, Bartol Research Institute, University of Delaware, Newark, DE 19716, USA.